Biochimica et Biophysica Acta 1812 (2011) 1041–1053

Contents lists available at ScienceDirect

Biochimica et Biophysica Acta

journal homepage: www.elsevier.com/locate/bbadis

Mitochondrial defect and PGC-1α dysfunction in *parkin*-associated familial Parkinson's disease ☆

Consiglia Pacelli [a], Domenico De Rasmo [a], Anna Signorile [a], Ignazio Grattagliano [b], Giuseppe di Tullio [c], Andria D'Orazio [c], Beatrice Nico [d], Giacomo Pietro Comi [e], Dario Ronchi [e], Ermanno Ferranini [f], Domenico Pirolo [f], Peter Seibel [g], Susanna Schubert [g], Antonio Gaballo [h], Gaetano Villani [a], Tiziana Cocco [a,*]

[a] *Department of Medical Biochemistry, Biology & Physics, University of Bari 'A. Moro', 70124 Bari, Italy*
[b] *Department of Internal Medicine and Public Medicine, University of Bari 'A. Moro', 70124 Bari, Italy*
[c] *Department of Translational Pharmacology, Consorzio Mario Negri Sud, Via Nazionale 8/A, 66030 Santa Maria Imbaro (CH), Italy*
[d] *Department of Human Anatomy and Histology, University of Bari 'Aldo Moro', 70124 Bari, Italy*
[e] *Dino Ferrari Centre, Department of Neurological Sciences, University of Milan, IRCCS Cà Granda Foundation Ospedale Maggiore Policlinico, 20122 Milan, Italy*
[f] *Department of Neurology, "Madonnina" Hospital, 70124 Bari, Italy*
[g] *Molecular Cell Therapy, Center for Biotechnology and Biomedicine, University of Leipzig, 04103 Leipzig, Germany*
[h] *Institute of Biomembranes and Bioenergetics, National Research Council (CNR), 70126 Bari, Italy*

ARTICLE INFO

Article history:
Received 22 November 2010
Received in revised form 23 December 2010
Accepted 24 December 2010
Available online 5 January 2011

Keywords:
Parkinson's disease
Parkin
Mitochondria
Oxidative stress
Peroxisome
PGC-1α

ABSTRACT

Mutations in the *parkin* gene are expected to play an essential role in autosomal recessive Parkinson's disease. Recent studies have established an impact of *parkin* mutations on mitochondrial function and autophagy. In primary skin fibroblasts from two patients affected by an early onset Parkinson's disease, we identified a hitherto unreported compound heterozygous mutation del exon2-3/del exon3 in the *parkin* gene, leading to the complete loss of the full-length protein. In both patients, but not in their heterozygous parental control, we observed severe ultrastructural abnormalities, mainly in mitochondria. This was associated with impaired energy metabolism, deregulated reactive oxygen species (ROS) production, resulting in lipid oxidation, and peroxisomal alteration. In view of the involvement of parkin in the mitochondrial quality control system, we have investigated upstream events in the organelles' biogenesis. The expression of the peroxisome proliferator-activated receptor gamma-coactivator 1-alpha (PGC-1α), a strong stimulator of mitochondrial biogenesis, was remarkably upregulated in both patients. However, the function of PGC-1α was blocked, as revealed by the lack of its downstream target gene induction. In conclusion, our data confirm the role of parkin in mitochondrial homeostasis and suggest a potential involvement of the PGC-1α pathway in the pathogenesis of Parkinson's disease. This article is part of a Special Issue entitled: Translating nuclear receptors from health to disease.

1. Introduction

Parkinson's disease (PD) is a chronic progressive neurodegenerative movement disorder characterized by the selective loss of dopaminergic neurons in the substantia nigra pars compacta.

While most cases of PD occur sporadically as the result of many different environmental factors, several gene products have been identified as responsible for Mendelian forms of PD. Autosomal dominant PD is caused by mutations in the leucine-rich repeat kinase 2 gene (LRRK2) [1] or in the α-synuclein gene [2]. The proteins implicated in autosomal recessive PD include parkin [3], PTEN-induced putative kinase 1 (PINK1) [4], DJ-1 [5] and ATP13A2 [6].

The evidence that these proteins are localized in mitochondria or are associated with the mitochondrial-dependent cell death would strengthen the hypothesis of mitochondrial oxidative dysfunction as the underlying alteration leading to PD development [7]. In particular, specific defects of complex I (CI) have been demonstrated in autoptic

Abbreviations: cAMP, cyclic adenosine monophosphate; CAT, catalase; CI, complex I; CII, complex II; CIV, complex IV; CV, complex V; CREB, cAMP-responsive element binding protein; CTRL, parental healthy control; DNP, dinitrophenol; GAPDH, glyceraldehyde-3-phosphate dehydrogenase; GPX, glutathione peroxidase; GSH, total glutathione; GSSG, oxidized glutathione; H_2DCFDA, 2′-7′dichlorodihydrofluorescin diacetate; LRRK2, leucine-rich repeat kinase 2; MCAD, medium-chain acyl-CoA dehydrogenase; MPTP, 1-methyl-4,1,2,3,6-tetrahydropyridine; NRF, nuclear respiratory factor; OXPHOS, oxidative phosphorylation system; P-CREB, phosphorylated-CREB; PD, Parkinson's disease; PGC-1α, peroxisome proliferator-activated receptor gamma-coactivator 1-alpha; PINK1, PTEN-induced putative kinase 1; RER, rough endoplasmic reticulum; SOD, superoxide dismutase; TBARs, thiobarbituric acid-reactive compound; TFAM, mitochondrial transcription factor A; TMPD, N,N,N′,N′-tetramethyl-p-phenylenediamine

☆ This article is part of a Special Issue entitled: Translating nuclear receptors from health to disease.

* Corresponding author. Department of Medical Biochemistry, Biology & Physics, Piazza G. Cesare, 11, 70124 Bari, Italy. Tel.: +39 080 5448537; fax: +39 080 5448538.
E-mail address: cocco.t@biochem.uniba.it (T. Cocco).

0925-4439/$ – see front matter © 2011 Elsevier B.V. All rights reserved.
doi:10.1016/j.bbadis.2010.12.022

specimens from the frontal cortex, platelets, skeletal muscle and cell cybrids from PD patients [8]. Substantial evidence supports the hypothesis that oxidative stress plays a major role in PD pathogenesis [9,10] conditions that, in dopaminergic neurons, could be amplified by the oxidative metabolism of dopamine [11] and the high levels of aerobic energy demand.

Since the discovery of mutations in the *parkin* gene (PARK2) as a cause of autosomal recessive juvenile parkinsonism [3], almost half of all PD cases have been associated with mutations in this gene. Parkin is a multifunctional E3 ubiquitin ligase, which mediates ubiquitylation of several target proteins [12]. A link between parkin and mitochondria was originally suggested by the observation that parkin prevents cytochrome *c* release in ceramide-treated cells [13]. Several studies on *parkin*-null animal models strongly suggest an important role of the *parkin* gene for the preservation of mitochondrial function. Despite having only mild deficits, *parkin* knockout mice exhibit mitochondrial dysfunction and oxidative damage [14,15] and *Drosophila parkin* null mutants display mitochondrial pathology and apoptotic muscle degeneration [16,17]. Functional assays in leukocytes [18] as well as fibroblasts of patients with *parkin* mutations [19–21] consistently show mitochondrial impairment. Recently, increasing experimental evidence reveal that parkin interacts with PINK1 in a common pathway regulating mitochondrial dynamics [22]. Moreover, it can induce proteasome-independent ubiquitylation which serves for a remarkably wide range of physiological functions [23,24], such as membrane protein trafficking and autophagy [25]. Parkin is recruited to depolarized mitochondria, through direct phosphorylation by PINK1, to mediate their autophagic degradation [26]. Furthermore, parkin has emerged as an important factor in the mitochondrial quality control mechanisms [27], where a fine balance of mitochondrial autophagy and biogenesis plays a key role in healthy mitochondrial network [28]. It has been reported that, in proliferating cells, parkin modulates basic mitochondrial functions and biogenesis through transcription/replication of mitochondrial DNA and protection of mitochondrial genomic integrity from oxidative stress [29]. A central role in a regulatory network involved in the transcriptional control of mitochondrial biogenesis and respiratory function is played by PGC-1α, a multifunctional protein found at higher levels in tissues with high metabolic requirement [30]. PGC-1α has emerged, in addition, as a key factor in the induction of many antioxidant programs in response to oxidative stress, in particular in neurons [31]. Several studies focus on the implication of PGC-1α in the pathogenesis of neurodegenerative diseases and open the possibility that modulation of PGC-1α activity could be of therapeutic interest in these disorders.

In the present study we have carried out a detailed genetic and biochemical analysis on primary skin fibroblasts from two sisters affected by an early onset PD, carrying mutations in *parkin* gene that cause a complete protein loss. Our analysis shows mitochondrial dysfunction associated with oxidative stress and altered PGC-1α function leading to transcription deregulation of target genes.

2. Materials and methods

2.1. Patients

We have examined an Italian family composed of four siblings, three of which show a juvenile form of PD. Diagnosis of PD was made according with the UK Brain Bank criteria: patients underwent neurological examination including the Unified Parkinson's Disease Rating Scale (UPDRS) and Hoen–Yahr Scale. The proband, a 36 year old man, showed an initial stiffness of the left leg at age 24 and over a few years, a camptocormic posture and a sporadic rest tremor of the left hand. At age 30, he had a moderate bradykinesia, symmetrical rigidity, a sporadic left hand rest tremor and a mild amimia. Cerebellar signs, a Babinski sign, supranuclear gaze palsy, autonomic involvement and/or cognitive deficit were absent (UPDRS scale 17). The two probands' female siblings that were analyzed are denominated P1 and P2 and the latter, twin sister of the proband, shows greater disease severity. Both siblings, first, showed a bradykinesia at age 35 (P1) and 31 (P2), followed, one year later, by a symmetrical rigidity and mild amimia. Cerebellar, pyramidal, oculomotoric, autonomic and cognitive dysfunction were absent (UPDRS scale 15 in P1 and 17 in P2 patients). Clinical response to dopaminergic treatment was excellent in the proband, while moderate in both sisters. The study was approved by the local Ethical Committee.

2.2. Genetic analysis of PD genes

After informed consent was obtained, total DNA was isolated from 3 ml peripheral blood with Iso Quick Nucleic Acid Extraction Kit (ORCA Research). The exons of PARK1 (α-synuclein), PARK2 (parkin), PARK6 (PINK1), PARK7 (DJ1) and PARK8 (LRRK2), were amplified by polymerase chain reaction (PCR). Primer pairs for amplification and sequencing have been previously described [2–5,32]. PCR reactions were purified using the ExoSAP-IT clean up method (Amersham Biosciences). Direct sequencing of both strands was done with Big Dye Terminator Cycle Sequencing Kit.

2.3. Reverse transcription (RT)-PCR and sequencing

Purification of total RNA from fibroblasts was carried out using RNeasy Mini Kit (Qiagen), according to the manufacturer's protocol. One microgram of total RNA was then reverse-transcribed to generate cDNA for PCR by using iScript cDNA Synthesis Kit (Bio-Rad). The *parkin* cDNA was amplified with the following PCR primers: sense 5′-TGGAGGATTTAACCCAGGAG-3′ and antisense 5′-ACAGGGCTTGGTG-GTTTTCT-3′. The PCR cycling protocol consisted of 30 cycles of denaturation at 94 °C for 1 min, annealing at 55 °C for 1 min and an extension at 72 °C for 1 min. PCR products were gel purified using the QIAquick Gel Extraction Kit (Qiagen) according to the manufacturer's instructions and then sequenced at PRIMM srl (Biomedical Science Park S. Raffaele, Milan, Italy).

2.4. Skin fibroblasts and culture conditions

Primary fibroblasts from the two siblings (P1, 36 years old, and P2, 32 years old) and the mother (parental healthy control, CTRL, 59 years old), were obtained by explants from skin punch biopsy, after informed consent. Control fibroblasts (NHDF AD, 56 years old) were purchased from American Type Culture Collection (ATCC; Virginia, USA). Cells were grown in high-glucose Dulbecco's modified Eagle's medium (DMEM) supplemented with 10% (v/v) fetal bovine serum (FBS), 1% (v/v) L-glutamine, 1% (v/v) penicillin/streptomycin, at 37 °C in a humidified atmosphere of 5% CO_2. All experiments were performed on cells with similar passage numbers, ranging from 5 to 14, to avoid an artifact due to senescence, known to occur at passage numbers greater than 30. In the passage range used, fibroblasts were β-Gal negative [33].

Where indicated, CTRL, P1 and P2 cells were grown in DMEM lacking glucose supplemented with 10% dialyzed FBS, 0.5 mg/l sodium pyruvate, 0.9 mg of galactose/ml.

2.5. Electron microscopy

Cells at 80% of confluence were collected by trypsinization and centrifugation, fixed in 3% glutaraldehyde, 0.1 M sodium phosphate buffer (pH 7.4) for 2 h, washed with the same buffer and subsequently fixed in 1% OsO_4 at 4 °C. Next, cells were dehydrated in graded ethanol, and embedded in Epon 812. Ultrathin sections (60 nm) were cut with a diamond knife on a LKB-V ultratome, stained with uranyl acetate followed by lead citrate and examined under a Zeiss EM 109

electron microscope (Zeiss, Oberkochen, Germany). Digital images were obtained with a cooled camera Gatan CMS (Gatan GmbH, München, Germany) and analyzed using Adobe Photoshop software (Adobe Systems, Inc. San Jose, CA, USA).

2.6. Measurement of endogenous respiration rates in intact cells and substrate-supported respiration rates in digitonin-permeabilized cells

Mitochondrial oxygen consumption was measured polarographically with a Clark-type oxygen electrode in a water-jacketed chamber (Hansatech Instruments, Norfolk, UK), magnetically stirred at 37 °C essentially as previously described [34,35].

For the measurement of respiration rates by endogenous substrates in intact cells, exponentially growing cells, fluid changed 1 day before the assays, were collected by trypsinization, and centrifugation and resuspended at $0.5–2\times10^6$ cells/ml in TD Buffer (0.137 M NaCl, 5 mM KCl, 0.7 mM Na_2HPO_4, 25 mM Tris–HCl, pH 7.4). Cell suspension was transferred to the polarographic chamber while an aliquot was used for cell counting and protein determination. After slope measurement, the coupled endogenous respiration was inhibited by 0.5 μg/ml oligomycin followed by 30 μM dinitrophenol (DNP).

For the measurement of respiration rates by exogenous substrates in digitonin-permeabilized cells, after full uncoupling of the endogenous respiration of intact cells with 30 μM DNP, digitonin was added directly into the oxygraphic chamber at the optimal concentration of 30 μg/10^6 cells [36]. After 2 min, respiratory substrates and inhibitors were added at the following concentrations: glutamate (5 mM)/malate (5 mM), succinate (5 mM) in the presence of 200 nM rotenone and ascorbate (10 mM) + N,N,N′,N′-tetramethyl-p-phenylenediamine (TMPD) (0.4 mM) in the presence of 13 nM antimycin A for Complex I (CI)-, Complex II (CII)- and Complex IV (CIV)-driven respiration, respectively. Intactness of the outer mitochondrial membrane was confirmed by the lack of further stimulation of respiration, upon addition of ferricytochrome *c* [37].

Since light microscopy of the cell monolayer revealed that patients' cells were larger than CTRL cells (data not shown) and that the specific cellular protein content was 2 and 3 fold higher in P1 and in P2, respectively, vs CTRL fibroblasts, all rates of oxygen consumption were normalized to cellular protein content [37].

2.7. OXPHOS enzymes and citrate synthase activity measurements

Cells, collected by trypsinization and centrifugation, were resuspended in hypotonic medium (25 mM potassium phosphate, pH 7.2, 5 mM $MgCl_2$), supplemented with the antiprotease cocktail tablet (Roche, Basel, CH). In order to allow complete accessibility of substrates to the inner mitochondrial membrane enzymes, samples were freeze–thawed three times, gently shaken and then resuspended in the assay buffer. CI (NADH:ubiquinone oxidoreductase, rotenone sensitive), CII (succinate-CoQ oxidoreductase, malonate sensitive), CIV (cytochrome *c* oxidase, KCN sensitive) and citrate synthase activities were measured spectrophotometrically with a Beckman DU7400 equipped with a rapid-mixing apparatus at 30 °C essentially as previously described [38]. ATP-hydrolase activity of Complex V (CV) (oligomycin sensitive) was measured on cell lysate as previously described [39].

2.8. Oxidative phosphorylation capacity and cellular ATP level measurements

The rate of mitochondrial ATP synthesis was determined in digitonin-permeabilized fibroblasts, collected by trypsinization and centrifugation and resuspended at $0.5–2\times10^6$ cells/ml in Buffer A (75 mM sucrose, 5 mM KH_2PO_4, 40 mM KCl, 0.5 mM EDTA, 3 mM $MgCl_2$, 30 mM Tris–HCl, pH 7.4) supplemented with 10 mM glucose, 38 U/ml esokinase and 0.3 mM P1,P5-di(adenosine-5′)pentaphosphate (Ap5A), as an inhibitor of adenylate kinase. Aliquots were used for cell counting and protein determination. After addition of digitonin (30 μg/10^6 cells), ATP synthesis was measured at 37 °C in the presence of 0.5 mM ADP using glutamate (5 mM)/malate (5 mM) or succinate (5 mM) *plus* 200 nM rotenone as respiratory substrates. After recording the state III respiration rates for 15 min, the reaction was stopped with 30% (v/v) perchloric acid. Debris was removed by centrifugation and samples, neutralized with 60% (v/v) KOH, were spectrophotometrically assayed for ATP content following the reduction of NADP induced by glucose-6-phosphate dehydrogenase. Steady-state cellular ATP levels were determined in digitonin-permeabilized cells in basal conditions or after 1 h pre-treatment with 100 μM iodoacetic acid as described above.

2.9. Lactate level and lactate dehydrogenase (LDH) activity measurements

Cells were seeded in 60 mm plastic Petri dishes and cultured for 48 h. The amount of lactate in the cell medium was estimated as described in [40]. LDH activity was measured spectrophotometrically on total cell lysates at 25 °C by following NADH oxidation at 340 nm in 50 mM Tris-HCl pH 7.4, 2 μg/ml rotenone and 0.1 mM NADH**.** The assay was started by adding 5 mM pyruvate.

2.10. Mitochondrial and peroxisomal labeling and confocal microscopy

For mitochondrial network analysis the cells were stained with Quant-iT™ PicoGreen® dsDNA reagent (Invitrogen, Molecular Probes) and MitoTracker®Red CMXRos (Invitrogen, Molecular Probes). Transient transfections with pDsRed2-Peroxi (staining peroxisomes) and pEGFP-N1 (staining cytoplasm)/pEGFP-Mito (staining mitochondria) were performed using FuGENE®HD (Roche, Basel, CH) and TransIT®-LT1 (Mirus, Madison, USA) according to manufacturer's conditions. Living cells cultured for 2 days on glass bottom dishes (MatTek Corporation Ashland) were analyzed with the inverted confocal laser scanning microscope TCS SP5 (Leica Microsystems). To avoid a cross talk in excitation of multiple stained compounds a sequential scanning mode was used. Images were acquired with photo multipliers and micrographs were processed and analyzed with the software Leica Application Suite Advanced Fluorescence 2.0.0, Adobe Photoshop CS and Huygens Professional 3.4.0p1.

2.11. Real-time PCR

RTqPCR on cDNA were performed essentially as previously described [41]. Quantitative normalization of cDNA in each sample was performed using glyceraldehyde-3-phosphate dehydrogenase (GAPDH), β-actin and 18S rRNA as internal control. Validated primers for real-time PCR are reported in the Supplemental materials.

2.12. Intracellular ROS measurements

Intracellular ROS level was determined using the cell permeant probe 2′-7′dichlorodihydrofluorescin diacetate (H_2DCFDA) [42]. Cells were incubated with 10 μM H_2DCFDA in a serum free medium in the dark at 37 °C for 30 min, collected by trypsinization, washed and resuspended in an assay buffer (100 mM potassium phosphate, pH 7.4, 2 mM $MgCl_2$). An aliquot was used for protein determination. The ROS-dependent oxidation of the fluorescent probe (507 nm excitation and 530 nm emission wavelength) was measured by a Jasco FP6200 spectrofluorimeter.

2.13. Antioxidant enzymes activities measurements

Measurements of antioxidant enzyme activities were carried out on cell lysates resuspended in hypotonic medium supplemented with the antiprotease cocktail tablet (Roche, Basel, CH), followed by a sonication step. Glutathione reductase, glutathione peroxidase (GPX) and catalase activities were assayed spectrophotometrically essentially as previously described [43]. Superoxide dismutase (SOD) activity was determined by using a native-gel activity-stain [44]. MnSOD was distinguished from cyanide-sensitive Cu/ZnSOD, by the addition of 2 mM KCN. Band intensity relative to the in-situ activity staining gels was calculated densitometrically using Quantity One-4.4.1 imaging software (Bio-Rad Laboratories). Silver staining of three replicate gel was used to verify equal loading.

2.14. Biochemical markers of oxidative stress

Cells, collected by trypsinization and centrifugation, were resuspended in hypotonic medium supplemented with the antiprotease cocktail tablet (Roche, Basel, CH) at a concentration of 1.5–2.0 mg protein/ml and homogenized with a glass/glass potter. Total glutathione (GSH), oxidized glutathione (GSSG) and protein sulfhydryl groups were measured as previously described [38]. For protein carbonyl (PC) determination, cellular proteins (1 mg) were precipitated with 10% TCA (w/v) and centrifuged. The pellet was resuspended in 1 ml of 0.2% (w/v) dinitrophenyl-hydrazine (DNPH) in 2N HCl or in 1 ml of 2N HCl, as a control blank, and processed [45]. The steady-state level of the lipid peroxidation product malondialdehyde (MDA) was assayed in cell lysates by determining thiobarbituric acid-reactive compounds (TBARs), spectrophotometrically at 532 nm [46].

2.15. Western blot analysis

Total cell proteins (30 μg) were separated on a 13% Tris–Tricine SDS-PAGE according to [47] and transferred onto nitrocellulose membrane. Western blot analysis was performed using the specified primary antibodies against: CI-39 kDa subunit, CIII-Core 2 subunit, CIV-Cox IV subunit, CV-β subunit and porin (Invitrogen), catalase (Calbiochem), cyclic AMP-responsive element binding protein (CREB) and phosphorylated-CREB (P-CREB) (Santa Cruz Biotechnology) according to the manufacturer's suggested concentrations. Protein loading was assessed by reprobing the blots with β-actin (Sigma) or GAPDH (AbD Serotec) monoclonal antibodies. Proteins were detected by chemiluminescent LiteAblot reagent (Euroclone) and the signal was quantified by densitometric analysis using Quantity One-4.4.1 imaging software (Bio-Rad Laboratories). For the parkin western blot analysis, 40 μg whole cell lysate proteins were separated on a 4–12% Tris–Tricine SDS-PAGE. Monoclonal parkin primary antibody (Sigma) was used according to the manufacturer's suggested concentrations. For the PGC-1α western blot analysis, 60 μg whole cell lysate proteins resuspended in RIPA buffer (50 mM Tris, pH 7.5, 1% Nonidet P-40, 150 mM NaCl, 1 mM EDTA, 0.1 % SDS, 0.5% Na-deoxycholate, protease inhibitor mixture (Roche, Basel, CH)) were separated on a 9% Tris–Glycine SDS-PAGE. Polyclonal PGC-1 α primary antibody (Santa Cruz Biotechnology) was used according to the manufacturer's suggested concentrations.

2.16. Mitochondrial protein synthesis

Fibroblast cell cultures from CTRL, P1 and P2 patients, after a 16 h incubation with 50 μg/ml of chloramphenicol, were washed three times with PBS and then labeled with 30 μCi [^{35}S]methionine-[^{35}S] cysteine for 2 h, in the presence of 100 μg/ml of emetine, in methionine-free DMEM supplemented with 10% dialyzed FBS. The cells were collected by trypsinization and centrifugation, washed twice with TD buffer and then resuspended in 50 μl TD supplemented with the antiprotease cocktail tablet (Roche, Basel, CH). Proteins (60–70 μg) of cell suspensions were separated on a 14% Tris–Glycine SDS-PAGE. The gel was dried and analyzed by PhosphorImager (Bio-Rad). Protein loading was assessed by immunoblot analysis of equal amounts of proteins using β-actin monoclonal antibody.

2.17. Cyclic adenosine monophosphate (cAMP) assay

For cAMP assay, the culture medium was removed and 1 ml of 0.1 M HCl was added to the cell layer followed by 10 min incubation at 37 °C. The lysed cells were scraped and transferred into Eppendorf tubes. The samples were centrifuged at 1300×*g* for 10 min at 4 °C. The supernatants were used for cAMP measurement using a direct immunoassay kit (Assay Designs) according to the manufacturer's instruction.

2.18. Statistical analysis

Data are expressed as means ± SEM and statistically analyzed by the Student's *t* test.

3. Results

3.1. Mutation analysis

A first screening of coding sequences of the genes known to be associated with autosomal recessive PD (PARK2, PARK6, PARK7) and of genes associated with autosomal dominant PD (PARK1 and PARK8) did not reveal any alteration in both P1 and P2 patients (data not shown). Since standard genomic sequencing may fail to detect compound heterozygous deletional mutations, RT-PCR was used to characterize the *parkin* gene as previously described [48]. The expected RT-PCR product of 1355 bp was present in the parental control (CTRL) and in the commercially available NHDF AD control fibroblasts, but it was absent in both patients (Fig. 1A). On the other hand, two bands, F1 (950 bp) and F2 (1191 bp) were detected in both patients, with the F1 being detectable also in the parental CTRL (Fig. 1A). Direct sequencing of the F1 and F2 RT-PCR products revealed a deletion of exons 2–3 and exon 3, respectively. Therefore, both patients carry a compound heterozygous deletional mutation (del exon2-3/del exon3), while the unaffected parental control displays the heterozygous del exon2-3 (Fig. 1B). The western blot analysis of parkin protein expression revealed the complete absence of the 50 kDa full-length protein in the fibroblasts of both patients and a comparable amount in CTRL fibroblasts and NHDF AD (Fig. 1C).

3.2. Ultrastructural analysis of cultured fibroblasts

Electron microscopy was used to examine ultrastructural differences between CTRL, P1 and P2 fibroblasts. As shown in Figures 2 (A–C), CTRL fibroblasts occur as elongated cells with thin plasma membrane filopodia, eucromatic nuclei and abundant rough endoplasmic reticulum (RER) with amorphous material filled cisternae. Numerous rounded or rod-like mitochondria normally arranged, with both lamellar and tubular cristae, lysosomal vacuoles and peroxisome-like bodies with uniform and moderately electron dense matrix were also scattered in the CTRL cytoplasm. Fibroblasts from both P1 and P2 patients (D–R) showed severe ultrastructural alterations, without morphological differences between each other, characterized by an irregular cellular shape with pseudopodia membranes and cytoplasmic protrusions, and heterochromatic and indented nuclei (Fig. 2D). Cytoplasm appeared electron lucent with abnormal enlargements of the cisternae of rough reticulum (Fig. 2O) and with numerous vesicles and lysosomal vacuoles completely (Figs. 2E,G,I arrow) or partially filled with electron dense material, possibly representing degenerating mitochondria (Figs. 2E,H,Q, arrowhead), and often merging with RER

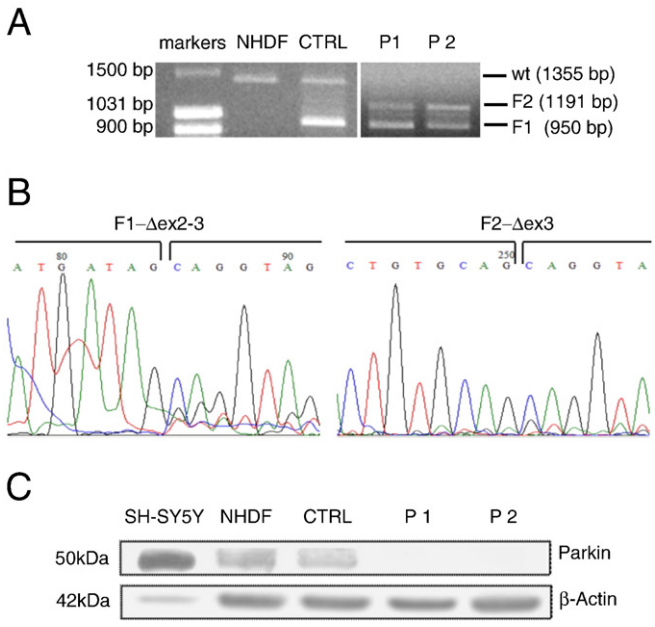

Fig. 1. Detection of compound heterozygous deletional mutations of *parkin*. (A) RT-PCR analysis of *parkin* gene was performed on cDNA obtained from NHDF AD fibroblasts (NHDF), patient 1 and 2 (P1, P2) and their parental control (CTRL) as described under Materials and methods. wt: full-length wild type product 1355 bp; F1: 950 bp fragment, exon2-3 deletion; F2: 1191 bp fragment, exon3 deletion. (B) Sequence chromatogram of the F1 fragment at the junction of the 3′ end of exon1 to the 5′ initial base of exon4 (F1-Δex2-3). Sequence chromatogram of the F2 fragment at the junction 3′ end of exon2 to the 5′ initial base of exon4 (F2-Δex3). (C) Western blot analysis reveals the presence of the parkin protein in NHDF and in CTRL fibroblasts, but not in the patient's cells (P1 and P2). Human dopaminergic neuroblastoma cell line (SH-SY5Y), was used as positive control for the expression of parkin protein and β-actin, as loading control.

cisternae (Figs. 2F,G, arrow). Lamellaries bodies (Fig. 2N, arrow), and peroxisome-like vacuoles, with a dense granular core (Figs. 2I,M asterisk), enveloped by lamellar structures (Fig. 2M, arrow), or irregularly patched dense matrix (Fig. 2L), were also detected. The most prominent abnormality, however, was represented by swollen mitochondria with few remaining cristae and decreased electron matrix density (Figs. 2O,P arrowhead) and degenerating with obscuration of the cristae and electron-dense matrices (residual bodies) (Figs. 2H,O,R, arrow) close to autophagic vacuoles containing mitochondrial membranes (Figs. 2Q,R, red arrow). No abnormal mitochondrial structures were present in CTRL fibroblasts.

In order to obtain further insights into the observed morphological mitochondrial defects, the mitochondrial networks of cultured cells were stained with MitoTracker CMXRos and a noticeably more fragmented mitochondrial network was exhibited by patients' fibroblasts in respect to CTRL (Fig. 3).

3.3. Functional analysis of bioenergetic metabolism

Next, we raised the question whether the marked changes in mitochondrial morphology may reflect alterations in mitochondrial function. The fibroblasts' competence for mitochondrial OXPHOS was first screened by monitoring cell growth rate in DMEM and in a selective medium containing galactose [49]. In high glucose-medium, patient's fibroblasts displayed a growth rate significantly lower with respect to the CTRL (Fig. 4A). However, while the growth curves of CTRL cells in glucose and galactose medium were superimposable, those of patients' fibroblasts showed a marked difference. In fact, the growth rate of P1 and, even more, of P2 fibroblasts was dramatically impaired in the galactose medium that forced the cells to use predominantly oxidative phosphorylation system (OXPHOS) for ATP synthesis, as compared with glucose medium (Fig. 4A). The mitochondrial respiratory function was then analyzed by measuring the oxygen consumption rates by endogenous substrates in intact cells. As shown in Figure 4B, the basal endogenous respiration rate in intact cells was significantly lower in P1 and P2 patients (47 ± 4.5% and 58 ± 3.9%, respectively) with respect to the CTRL fibroblast. Similarly, the maximal DNP-uncoupled respiration rates in P1 and P2 fibroblasts decreased by 56 ± 6.3% and 65 ± 2.5%, respectively, as compared with the CTRL value. In view of the marked age-related decline of fundamental processes essential for mitochondrial biogenesis and function in human fibroblasts [35], it should be stressed that the respiratory rates of both control cells (CTRL and NHDF AD cells) fall within the range of their age matched group. Furthermore, the ratio of the DNP-uncoupled vs the oligomycin-blocked respiration rate (data not shown), was lower in both patients' as compared with CTRL cells, suggesting a certain degree of uncoupling in both patients.

To further dissect the observed decrease in endogenous respiration, we measured the maximal (uncoupled) respiratory fluxes by exogenous substrates supplying electrons to CI (glutamate + malate), CII (succinate) or CIV (ascorbate + TMPD) in digitonin-permeabilized cells (Fig. 4C). A significant reduction of the uncoupled respiration rates was observed in both patients, independent of the substrate used, suggesting an overall reduction in the respiratory capacity of the electron transport chain. Respiratory fluxes were markedly decreased with respect to CTRL, by 41 ± 8.2%, 31 ± 6.5% and 25 ± 9.5% in P1, by 59 ± 3.3%, 50 ± 3.7% and 44 ± 4.3% in P2 using glutamate + malate, succinate and ascorbate + TMPD, respectively.

In order to investigate whether the observed decline of the respiratory fluxes in the patients was related to the impaired function of specific respiratory complexes, CI, CII and CIV activities were measured. As shown in Table 1, a highly significant decrease of CI activity in P1 (36.1 ± 7.1%) and P2 (28.4 ± 3.7%) and, although to a smaller extent, of CIV in P1 (10.2 ± 5.5%) and P2 (18.3 ± 8.3%) as compared to the CTRL ones, was found. On the other hand, the CII activity was not significantly changed in patients' cells vs CTRL. Interestingly, the activity of citrate synthase, a well-known functional marker of mitochondrial content, was also decreased by 44 ± 4.5% and 38 ± 5.5% in P1 and P2, respectively, as compared to CTRL.

The OXPHOS capacity of both patients' fibroblasts was also examined by measuring the coupled state III respiration rate (in the presence of ADP) and cellular ATP production rate in permeabilized cells. Consistent with the results described above, we observed lower respiration rates in P1 and P2 fibroblasts with NAD-dependent substrates and with succinate as compared with the control values (Fig. 4D). The oligomycin-sensitive ATP synthesis rates sustained by glutamate + malate and succinate were decreased by 51 ± 7.8% and 59 ± 5.9% in P1 and by 80 ± 3.3% and 71 ± 5.2% in P2, respectively as compared with CTRL cells (Fig. 4E). Moreover, the oligomycin-sensitive ATP hydrolase activity of CV also revealed a noteworthy decrease in both patients as compared to the CTRL value (data not shown).

Despite a defective OXPHOS, the cellular total ATP content, measured under basal conditions, was significantly higher in P1 (24 ± 9.2%) and in P2 (65 ± 5.6%) compared with CTRL values (Fig. 4F). Similar results were obtained by measuring the ATP content under strict glycolytic conditions, i.e. in the presence of antimycin A and rotenone (data not shown). On the other hand, cellular ATP content, in the presence of the glycolytic inhibitor iodoacetic acid, was decreased by 44 ± 1.04% and 40 ± 1.39% in P1 and P2 fibroblasts, respectively (Fig. 4F). These data indicate that the defective ATP production by OXPHOS in patients' fibroblasts is compensated by an increased glycolytic supply. Consistent with the increased glycolytic ATP production was the greater intracellular LDH activity (Fig. 4G) observed in P1 (71.3 ± 13.8 %) and in P2 (84.1 ± 12.9%) as compared with CTRL, as well as the higher extracellular lactate levels (Fig. 4H) which were increased by 33 ± 9.4% and 52 ± 12.1% in P1 and P2 fibroblasts, respectively, as compared with CTRL fibroblasts.

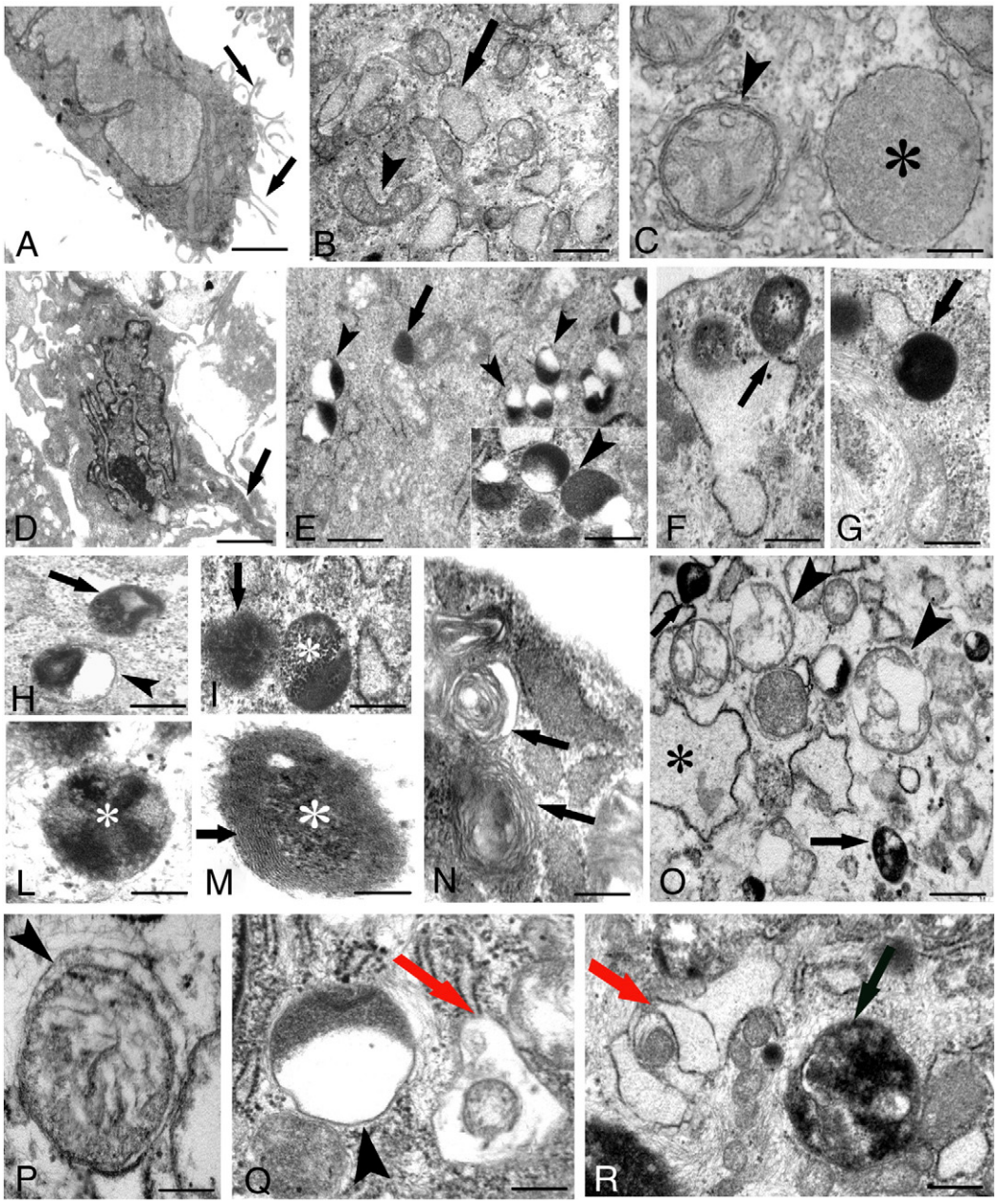

Fig. 2. Ultrastructural analysis of skin fibroblasts. (A–C) Representative micrographs of fibroblasts from CTRL showing eucromatic nucleus and filopodia (A, arrow), RER with dilated cisternae (B, arrow), mitochondria with lamellar (B, arrowhead) and tubular cristae (C, arrowhead) and lysosomes with uniform matrix (C, asterisk). (D–R) Representative micrographs of fibroblasts from P1 and P2 patients showing pseudopode membrane (D, arrow), indented nucleus with enlarged RER cisternae (O, asterisk) and lysosomal vacuoles completely (E, G, I, arrow) or partially filled with electron dense material (E, H, Q, arrowhead), merging with RER cisternae (F, G, arrow). Lamellaries bodies (N, arrow) and peroxisome-like vacuoles showing granular core (I, M, asterisk), enveloped by lamellar structures (M, arrow), or patched dense matrix (L, asterisk) are detectable. Swollen mitochondria with disorganized membrane compartments (O, P, arrowhead) and degenerating with electron-dense matrices (H, O, R, arrow) close to autophagic vacuoles containing mitochondrial membranes (Q, R, red arrow) are present. Scale bar: A, D, 0.83 μm; B, E, O, 0.5 μm; E inset, F, G, H, I, N, Q, 0.2 μm; C, L, M, P, 0.11 μm.

3.4. Oxidative stress analysis

Mitochondrial dysfunction is often associated with an increased ROS production, therefore we have evaluated the production of ROS by measuring the oxidation of H_2DCFDA in patients and CTRL cells. As shown in Figure 5A, a significant increase in ROS production by 31 ± 9.9% and 53 ± 13.8% in P1 and P2 cells, respectively, was observed as compared with CTRL ones.

These results prompted us to investigate levels of oxidative stress markers. The content of protein carbonyls and TBARs, as protein and lipid oxidative damage markers, respectively, are shown in Figures 5B and C. When compared with CTRL, the total level of protein carbonyl did not differ significantly in PD patients' fibroblasts (Fig. 5B), whereas higher TBARs were detected in P1 (52.6 ± 8.3%) and P2 (47.4 ± 5.9%) (Fig. 5C). No significant difference was observed in the cellular content of GSH, GSSG and protein sulfhydryl groups (data not shown).

The differences in the ROS levels observed in the patients' cells could be also due to deficiencies in the scavenging apparatus. For these reasons, the activity of the antioxidant enzymes was analyzed. Fibroblasts of both patients exhibited a decreased activity of mitochondrial MnSOD (Fig. 5D) (31.6 ± 4.7% in P1, 44.4 ± 13.6% in P2), GPX (Fig. 5E) (30.9 ± 9.9% in P1, 54.5 ± 4.2% in P2) and catalase (Fig. 5F) (53.2 ± 5.7% in P1, 31.9 ± 4.8% in P2) compared to CTRL cells. No significant change in glutathione reductase activity was observed (data not shown). As shown in Figure 5G, the reduction of the catalase activity was due to a lower protein level which was decreased by 52.9 ± 4.7%

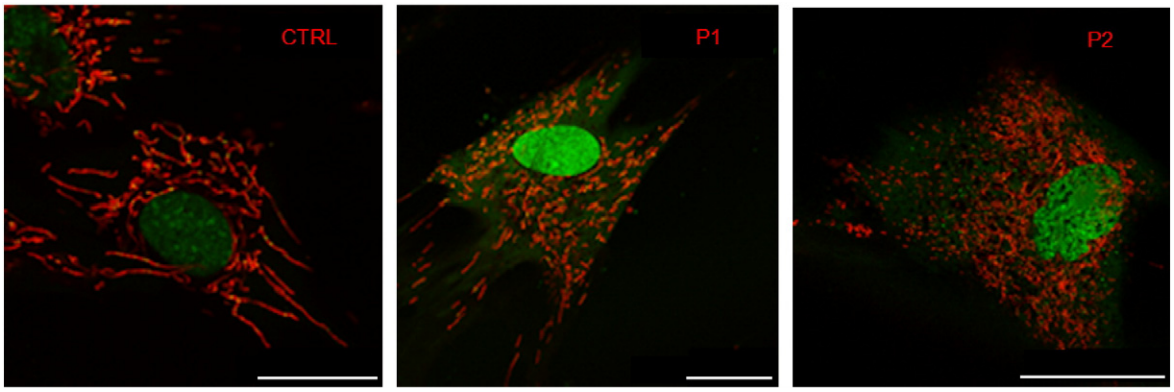

Fig. 3. Mitochondrial network analysis. Representative confocal images of mitochondrial network in fibroblasts from CTRL (scale bar: 25 μm), P1 (scale bar: 25 μm) and P2 (scale bar: 50 μm) patients, stained with nuclear stain (green) and mitochondrial stain (red) as described under Materials and methods.

and 53.1 ± 9.2% in P1 and P2, respectively, as compared to CTRL fibroblasts.

Finally, to test whether the decrease of catalase could be associated with a decreased peroxisome content, total peroxisome volume quantification was analyzed. The analysis revealed, unexpectedly, that P1 and P2 fibroblasts contain about a 5–6 fold increase of peroxisome volume (normalized to cell volume) when compared to CTRL (Fig. 6).

3.5. Mitochondrial biogenesis and PGC-1α dysfunction

To assess whether an altered expression of mitochondrial proteins could underlie the reduction in the respiratory chain complex activities observed in both patients, we evaluated, by semi-quantitative western blotting analysis, the steady-state levels of different OXPHOS subunits (Fig. 7A). The results showed a significant decrease in the expression level of CI, CIII, CIV and CV subunits as well as of the mitochondrial outer membrane porin, in patients' fibroblasts with respect to the CTRL cells. The synthesis of mitochondrial-encoded proteins, measured by the incorporation of [^{35}S]-labeled methionine, appeared consistently decreased in P1 and P2 fibroblasts with respect to the CTRL (Fig. 7B). Mitochondrial dysfunction often elicits a compensatory increase in organelle biogenesis. PGC-1α is a transcriptional coactivator directly involved in the upstream control of mitochondrial biogenesis [50,51]. Several signal transduction pathways have been implicated in the control of PGC-1α expression and activity, among which is the cAMP mediated signal transduction pathways that results in phosphorylation of CREB [51]. Interestingly, we found a rise in the cAMP basal level (Fig. 7C), associated with an increase of P-CREB in respect to total CREB content in both patients, more marked in P2 (151.5 ± 44.7%) than in P1 (32.2 ± 12.2%) as compared to CTRL fibroblasts (Fig. 7D). In agreement with the results described above, PGC-1α expression appeared to be upregulated (Figs. 7E and F). The endogenous PGC-1α transcripts were 5.8-fold and 12.6-fold higher in P1 and P2 respectively, compared to CTRL (Fig. 7E). Consistently, the PGC-1α protein content was increased by 23.9 ± 7.4% in P1 and 85.5 ± 3.6% in P2 as compared with CTRL (Fig. 7F). Strikingly, the mRNA levels of PGC-1α downstream target genes, directly involved in mitochondrial biogenesis (NRF1, NRF2, TFAM, ATPaseβ, COX II), as well as, in fatty acid metabolism (MCAD), resulted to be generally unchanged or even significantly lower in both patients as compared with CTRL (Fig. 7G). The PGC-1α target genes for the antioxidant enzymes, GPX1 and SOD2, had likewise a significant lower expression (Fig. 7G). Comparable patterns for mRNA levels of PGC-1α and its target genes were obtained by using β-actin (Fig. 7G) and GAPDH or 18S rRNA (Fig. S1) as housekeeping genes.

4. Discussion

Recent research on PD-associated genes has provided a fundamental knowledge of biochemical pathways associated with the disease process. Moreover, genetic and toxin models suggest that mitochondrial dysfunction is a common denominator of sporadic and familial PD. In the present work, we have carried out an extensive analysis of mitochondrial bioenergetic properties of fibroblasts from two siblings with juvenile PD. The genetic analysis revealed a hitherto unreported compound heterozygous mutation del exon2-3/del exon3 in the *parkin* gene, leading to the complete loss of the full-length protein. The del ex2-3 mutation was harbored in heterozygosis in the patients' mother who did not present any pathological symptom (parental healthy control, CTRL). Although exon2-3 [52] and exon3 [53] deletional mutations in the *parkin* gene have been previously described, this is, to our knowledge, the first report of the two mutations appearing simultaneously in compound heterozygotes.

Whether heterozygous mutations in the *parkin* gene can cause parkinsonism or can confer an increased susceptibility for typical late-onset PD is still controversial [54–57]. The absence of any mitochondrial defect in the heterozygous parental control is in line with the evidence that the siRNA-mediated *parkin* 50% knockdown does not result in an impaired mitochondrial transmembrane potential nor in mitochondrial morphology alteration [20]. Mitochondrial defect has been primarily demonstrated by a specific impairment in growth of both patients' cells in a medium containing galactose, which is metabolized through the glycolytic pathway only very slowly [49].

The mitochondrial functions investigated in CTRL exhibited unchanged values with respect to the unrelated matched control. We provide evidence, in PD patients' fibroblasts, of significantly decreased respiratory capacities by endogenous and exogenous substrates in intact and permeabilized cells, respectively, as compared with the parental control, and even more with the average age-matched values (cf. [35]). The more evident decline of the maximal respiratory rates by NAD-dependent substrates and of the specific CI enzyme activity is in agreement with previous data obtained in peripheral cells from *parkin* patients [18] and in mouse *parkin* mutants model [14].

The inhibition of respiratory fluxes is also associated with a decline in CIV function as measured polarographically in intact (data not shown) and in digitonin-permeabilized cells and confirmed by the spectrophotometric assay of the specific CIV enzyme activity. A reduced capacity of the electron transport chain has been already reported in mouse models of PD, such as *parkin*$^{-/-}$ mice [14,15] and *pink1*$^{-/-}$ mice [58] as well as in fibroblasts derived from patients bearing *parkin* mutations [20]. The functional decline could be due to

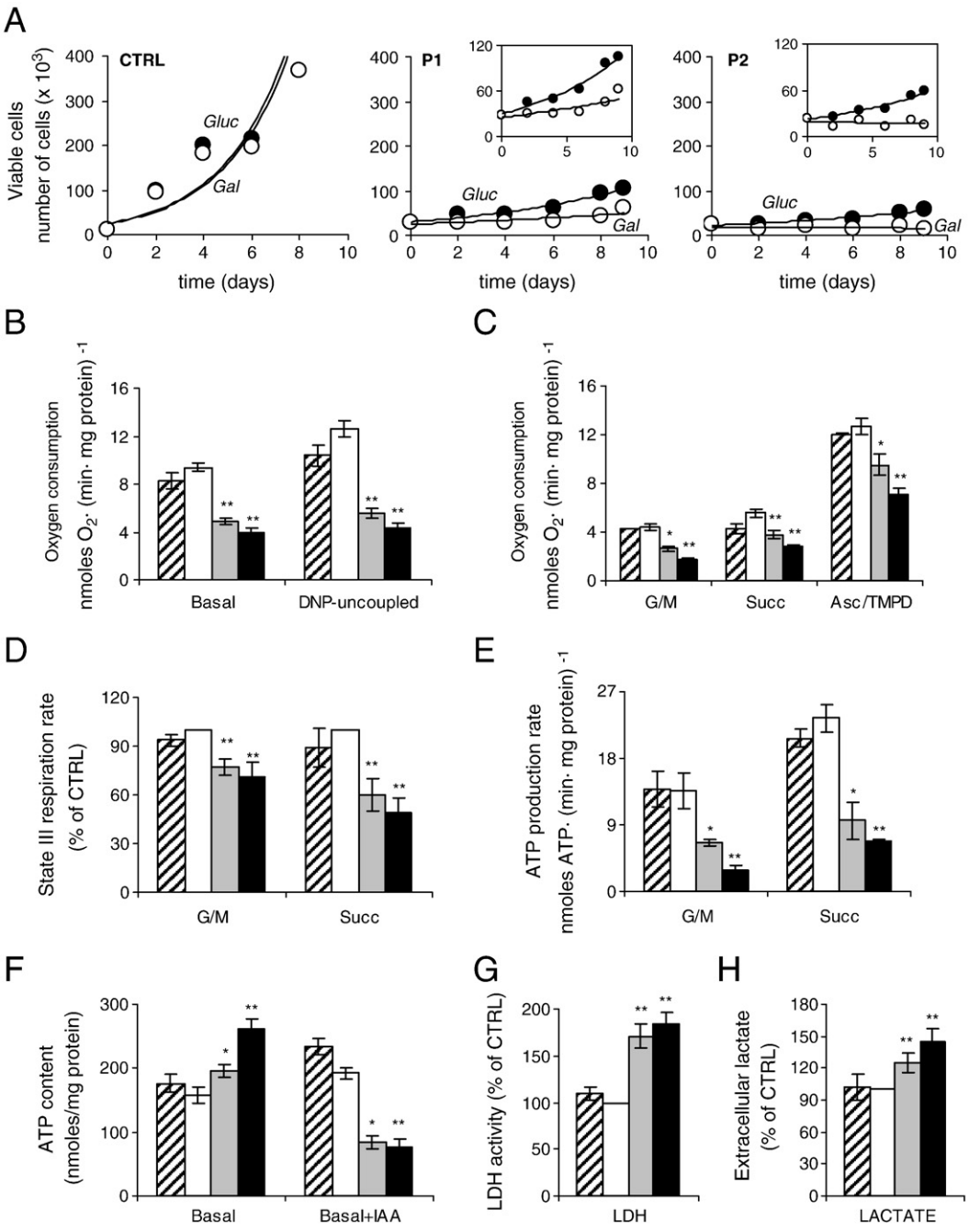

Fig. 4. Functional analysis of bioenergetic metabolism. (A). Cellular growth curves. Fibroblast growth was monitored in CTRL, P1 and P2 fibroblasts in standard *glucose*/medium (closed circle) or in *galactose*/medium, lacking glucose, and containing, 0.9 mg of galactose/ml and 0.5 mg of pyruvate/ml (open circle). (B) Basal and DNP (30 μM)-uncoupled endogenous respiration rates in intact cells. (C) DNP-uncoupled respiration rates in digitonin-permeabilized cells were measured in the presence of CI (G/M, glutamate 5 mM + malate 5 mM, rotenone sensitive fraction), CII (Succ, succinate 5 mM *plus* rotenone, antimycin A sensitive fraction) and CIV (Asc 10 mM/TMPD 0.4 mM *plus* antimycin A, cyanide sensitive fraction) substrates. (D) State III respiration rates were measured after addition of 0.5 mM ADP in the presence of glutamate + malate (G/M) or succinate *plus* rotenone (Succ) in digitonin-permeabilized cells. The values are expressed as percentage of CTRL whose mean values ± SEM are 4.9 ± 0.7 and 7.7 ± 0.6 nmoles $O_2 \cdot (\text{min} \cdot \text{mg protein})^{-1}$ for G/M and Succ, respectively. (E) Oligomycin-sensitive ATP synthesis rates were measured in the presence of CI (G/M), and CII (Succ) substrates in digitonin-permeabilized cells. (F) Cellular ATP content under basal conditions (Basal) and after treatment with 100 μM iodoacetic acid for 1 h (basal + IAA) was measured in digitonin-permeabilized cells. (G) LDH activity was measured in total cell lysates. Data are expressed as percentage of CTRL whose mean value ± SEM is 2.7 ± 0.1 μmoles $\cdot (\text{min} \cdot \text{mg protein})^{-1}$. (H) Extracellular lactate level was measured in the growth medium at 48 h after seeding. Data are expressed as percentage of CTRL whose mean value ± SEM is 105.2 ± 16.1 nmoles/μg protein. The values reported represent the means ± SEM of at least four independent experiments. For more details see Materials and methods. Hatched bar, NHDF AD; open bar, CTRL; gray bar, P1; filled bars, P2. $^{*}p<0.05$, $^{**}p<0.005$.

the decreased protein level of OXPHOS subunits reported in our work and also described in *parkin*$^{-/-}$ mice by Palacino et al. [14]. These results would highlight the involvement of *parkin* in the biogenesis of mitochondrial respiratory chain complexes [59].

The major harmful consequence of a defective electron transfer chain is displayed in ATP synthesis by OXPHOS. The decreased mitochondrial ATP synthesis by CI- and CII-substrates, observed in patients' fibroblasts, is compensated by an increase in the anaerobic glycolytic pathway. A general shift to anaerobic glycolysis in the neocortex of PD patients has been established by magnetic resonance spectroscopy and 2-[18F]fluoro-2-deoxy-D-glucose positron emission tomography studies, showing increased lactate concentrations [60].

Table 1
Mitochondrial respiratory enzyme and citrate synthase activities.

Enzyme activities (% CTRL)	NHDF AD	P1	P2
Complex I	95 ± 8	**64 ± 7	**72 ± 4
Complex II	119 ± 11	123 ± 10	107 ± 10
Complex IV	96 ± 8	*90 ± 6	*82 ± 8
Citrate synthase	87 ± 5	**56 ± 5	**62 ± 6

Specific enzymatic activities of mitochondrial respiratory chain CI, CII, CIV, and citrate synthase were measured on total cell lysates from NHDF AD, parental CTRL, and P1 and P2 fibroblasts as described under Materials and methods. Data are expressed as percentage of CTRL values. The mean values ± SEM for CI, CII, CIV and citrate synthase activities in CTRL fibroblasts were 34.7 ± 4.3, 10.5 ± 0.7, 13.2 ± 0.9, 20.5 ± 2.5 nmoles · (min · mg protein)$^{-1}$, respectively. The values represent the means ± SEM of at least four independent experiments. For more details see Materials and methods.
* $p<0.05$.
** $p<0.005$.

As expected, the defects in the electron transfer chain lead to an increase in ROS production. The resulting significant increase in TBARs detected in the patients' fibroblasts, strengthen the role of lipid peroxidation as the major link between parkin fibroblasts and PD substantia nigra [61]. Lipid peroxidation products are thought to be markers of early PD pathogenesis even before clinical manifestation, since abnormally high levels have been observed in brain autopsies of asymptomatic individuals [62] and in the substantia nigra of PD patients [63]. On the contrary, no oxidative protein damage and no change in cellular glutathione content was detected in patients' cells, suggesting their possible implication in a later phase of PD pathogenetic mechanisms (see however [64,65]). Finally, the observation of the significant decline of catalase, glutathione peroxidase and MnSOD activities in the patients' fibroblasts worsen the oxidative stress condition that is considered a common underlying feature in PD pathogenesis (see also [66,67]).

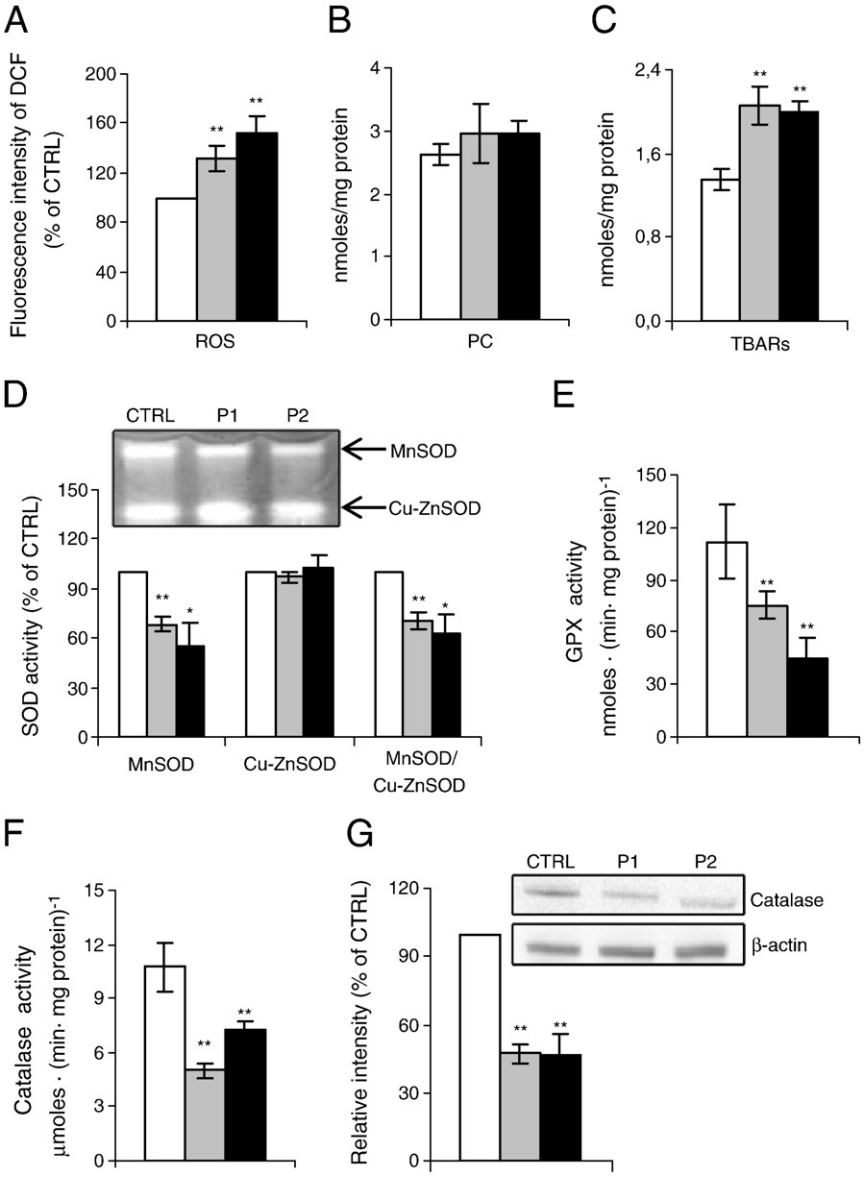

Fig. 5. Oxidative stress analysis. (A) The intracellular ROS content was detected by DCF fluorescence in cells loaded with DCFH-DA (10 µM) for 30 min. Data are expressed as percentage of CTRL values. Cellular content of (B) protein carbonyls (PC), and (C) thiobarbituric acid-reactive compounds (TBARs), were measured on total cell lysates. (D) Representative "in situ" SOD activity assay, determined by histochemical staining of a native-gel. Bar graph shows quantification of SOD positive bands by densitometric analysis. Data are expressed as percentage of CTRL values. (E) GPX and (F) catalase activities were measured in total cell lysates. (G) Representative western blot of catalase content performed on whole cell lysates. Bar graph shows quantification by densitometric analysis of band intensity of catalase normalized to β-actin, used as loading control. Data are expressed as percentage of CTRL values. For more details see Materials and methods. The values reported represent the means ± SEM of at least four independent experiments. Open bar, CTRL; gray bar, P1; filled bars, P2. *$p<0.05$, **$p<0.005$.

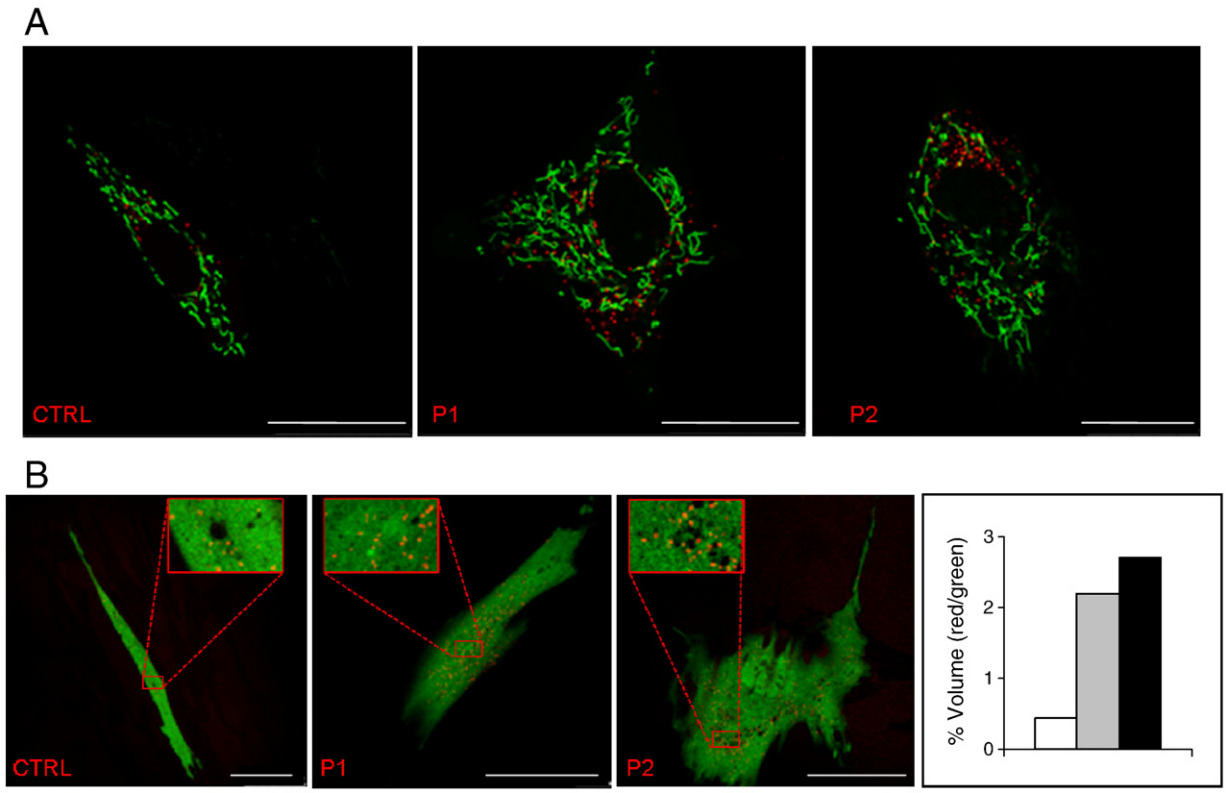

Fig. 6. Peroxisome volume analysis. (A) Representative confocal images of fibroblasts from CTRL (scale bar: 25 μm), P1 (scale bar: 25 μm) and P2 (scale bar: 25 μm) patients expressing mitochondrial (green) and peroxisomal (red) fluorescent fusion proteins. (B) Representative confocal images of fibroblasts from CTRL (scale bar: 50 μm), P1 (scale bar: 50 μm) and P2 (scale bar: 50 μm) patients expressing cytoplasmic (green) and peroxisomal (red) fluorescent fusion proteins. Bar graph shows ratio of peroxisome volume (red) and cell volume (green) quantification, obtained by confocal images reported in B, taken and processed by deconvolution software (background reduction). The images underwent pixel analysis and the corresponding values were acquired. Open bar, CTRL; gray bar, P1; filled bars, P2.

The brain is particularly vulnerable to oxidative stress since the high demand of a strictly aerobic energy production seems not to be balanced by an efficient antioxidant defense system as compared with other organs [68]. This scenario would become particularly dangerous in dopaminergic neurons where a pro-oxidant environment exists, due to the presence of dopamine. While the "vicious circle" between mitochondrial respiratory dysfunction and ROS production might be, somehow, expected, the decrease in the ROS scavenging system shifted our investigation in different directions. Of particular interest was, for us, the decrease of catalase activity and protein expression, and the increase in peroxisomal number observed in PD fibroblasts. Catalase exists primarily within peroxisomes and removes the H_2O_2 generated by the long-chain fatty acid beta-oxidation pathway. The enzyme deficiency might contribute to the imbalance of intracellular ROS, affecting lipid metabolism and membrane function. Furthermore, the peroxisomal generated H_2O_2 may move into the cytoplasm to induce an overall intracellular stress condition affecting organelles' function.

Recently, a close association between mitochondria and peroxisomes has been described [69]. Both organelles are in close contact with the endoplasmic reticulum, exchanging metabolites and sharing some metabolic pathways and components of their division machinery, so that their biogenesis can occur in a coordinated manner [69,70]. The interrelationship between the two organelles has been strengthened by the recent demonstration of a concerted action of PGC-1α on mitochondrial function and peroxisomal specialization and biogenesis [71]. Indeed, it has been shown that the increase of the peroxisomal catalase level in senescent human cells restores mitochondrial integrity [72] while its inactivation results in mitochondrial dysfunction and an increase in peroxisome number [73]. Alterations in peroxisomal metabolism, biogenesis, dynamics and proliferation can potentially influence mitochondrial functions and vice versa having a negative impact on their cooperative function, thus contributing to disease appearance [69] and aging process [74].

The morphological abnormalities that we observed in PD patients, mainly in mitochondria, would be the result of the mitochondrial dysfunctions and the oxidative stress condition so far described. In fact, current data suggest that parkin is required for the turnover of compromised mitochondria by promoting their autophagy [26,75,76], recruiting the autophagic adaptor protein p62 [77,78], a protein involved, also, in pexophagy [79]. The imbalance between the extent of autophagy induction and the ability of the cell to complete autophagic degradation and recycling/regeneration of cellular components, upregulating compensatory biosynthetic responses, would create a state of autophagic stress and eventually cell death [80].

In this scenario and in the light of the possible involvement of parkin in mitochondrial turnover [59], we have investigated upstream events in the organelles biogenesis. Several signal transduction pathways are implicated in the control of expression and activity of PGC-1α, a strong regulator of mitochondrial biogenesis, required, as well, for the induction of many ROS detoxifying enzymes upon oxidative stress [31]. Activation of the cAMP signaling pathway is a major mechanism underlying the induction of PGC-1α, whose promoter contains a functional CREB binding site that is required for cAMP response [51]. Abnormal PGC-1α activity likely plays an important role in the pathogenesis of several metabolic diseases [51] and it is rising its involvement in the pathogenesis of neurodegenerative disorder such as Huntington's disease [81,82] and Friedreich's ataxia [83]. Specifically related to PD is the evidence that a PGC-1α knockout mice shows enhanced susceptibility to neuronal loss following MPTP exposure [31]. Furthermore, during the preparation of this manuscript, Scherzer's group reported a reduced expression of PGC-1α target genes related to mitochondrial function

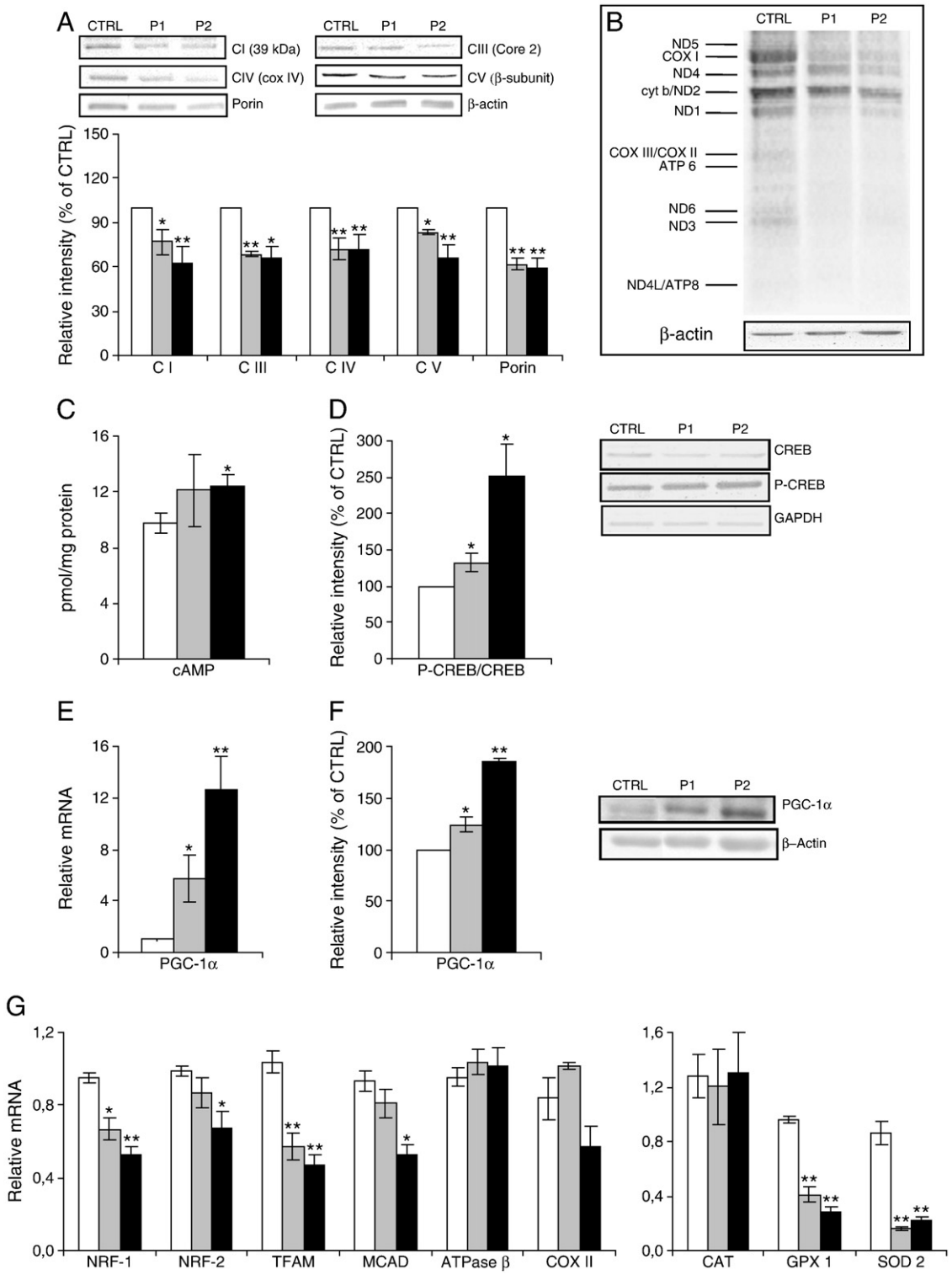

Fig. 7. Mitochondrial biogenesis and PGC-1α dysfunction. (A) Protein expression of respiratory chain complexes and of porin. Representative western blot of CI (39 kDa), CIII (core 2), CIV (Cox IV), CV (β-subunit) respiratory chain's subunits and of porin, performed on whole cell lysates. Bar graph shows quantification by densitometric analysis of mitochondrial protein bands normalized to β-actin, used as loading control. Data, means ± SEM of at least four independent experiments, are expressed as percentage of CTRL values. (B) [^{35}S]-methionine labeled mitochondrial protein synthesis. Representative autoradiographic patterns of mitochondrial translation. (C) cAMP basal levels in total cell lysates. Data are means ± SEM of at least three independent experiments. (D) Western blot of CREB and P-CREB, performed on whole cell lysates. Bar graph shows the CREB/P-CREB ratio calculated by quantification by densitometric analysis of band intensity normalized to GAPDH, used as loading control. Data are means ± SEM of at least four independent experiments, expressed as percentage of CTRL values (E) PGC-1α mRNA levels. The mRNA levels were determined by RTqPCR of total RNA normalized to GAPDH. Data are means ± SEM of at least four determinations. (F) Western blot of PGC-1α performed on whole cell lysates. Bar graph shows quantification by densitometric analysis of band intensity normalized to β-actin, used as loading control. Data are means ± SEM of at least three independent experiments, expressed as percentage of CTRL values. (G) mRNA levels of PGC-1α target genes: NRF1, NRF2, TFAM, ATPaseβ, COX II, MCAD and antioxidant enzymes CAT, GPX1, SOD2. The mRNA levels were determined by RTqPCR of total RNA normalized to GAPDH. Data are means ± SEM of at least four determinations. For more details see Materials and methods. Open bar, CTRL; gray bar, P1; filled bars, P2. $^{*}p<0.05$, $^{**}p<0.005$.

and energy production, in the substantia nigra and in non-nigral tissues of PD patients [84].

In our study, changes in cellular metabolism, due to the loss of mitochondrial oxidative capacity, could elicit an adaptive response by promoting a signaling pathway involving activation of CREB by phosphorylation, which is reported to be catalyzed by several kinases such as the cAMP-dependent Protein Kinase (PKA) [30]. CREB phosphorylation leads to the remarkable upregulation of PGC-1α expression which is, however, not associated with any increase in the transcript levels of its target genes. This fact would pinpoint to possible post-translational modifications known to modulate PGC-1α function such as phosphorylation, acetylation, methylation and sumoylation [85]. These modifications can affect the intrinsic activity and stability of PGC-1α or regulate its interaction with other proteins. In particular, the reversible acetylation by the NAD-dependent protein deacetylase sirtuin 1 (SIRT1) is emerging as a crucial controller of mitochondrial biogenesis [86] and autophagy [87].

5. Conclusion

In conclusion, this work strengthens the role of mitochondrial dysfunctions and oxidative stress in PD pathogenesis, highlighting the overall mitochondrial homeostasis impairment as causative of the pathological process. The compensatory increase of PGC-1α level is not associated with induction of its target genes thus failing to correct the mitochondrial defects as well as the oxidative stress condition. Involvement of PGC-1α in parkin-associated PD still require further studies routed to define the role of parkin in quality control of mitochondria and peroxisomes. Strategies to promote PGC-1α function could represent a promising therapeutic approach for the treatments of multiple forms of PD and other neurodegenerative disorders.

Supplementary materials related to this article can be found online at doi:10.1016/j.bbadis.2010.12.022.

Acknowledgments

We thank Salvatore Scacco for explants from a skin punch biopsy.

This work was supported by grants from the National Research Project (PRIN 2006 n° 2006069034_004) of the Italian Ministry for the University (MIUR) and from local funding from University of Bari to T.C. and G.V. This work was additionally supported in part by a grant of the Sächsische Ministerium für Wissenschaft und Kunst (SMWK) awarded to P.S.

References

[1] C. Paisan-Ruiz, S. Jain, E.W. Evans, W.P. Gilks, J. Simon, M. van der Brug, A. Lopez de Munain, S. Aparicio, A.M. Gil, N. Khan, J. Johnson, J.R. Martinez, D. Nicholl, I.M. Carrera, A.S. Pena, R. de Silva, A. Lees, J.F. Marti-Masso, J. Perez-Tur, N.W. Wood, A.B. Singleton, Cloning of the gene containing mutations that cause PARK8-linked Parkinson's disease, Neuron 44 (2004) 595–600.

[2] M.H. Polymeropoulos, C. Lavedan, E. Leroy, S.E. Ide, A. Dehejia, A. Dutra, B. Pike, H. Root, J. Rubenstein, R. Boyer, E.S. Stenroos, S. Chandrasekharappa, A. Athanassiadou, T. Papapetropoulos, W.G. Johnson, A.M. Lazzarini, R.C. Duvoisin, G. Di Iorio, L.I. Golbe, R.L. Nussbaum, Mutation in the alpha-synuclein gene identified in families with Parkinson's disease, Science 276 (1997) 2045–2047.

[3] T. Kitada, S. Asakawa, N. Hattori, H. Matsumine, Y. Yamamura, S. Minoshima, M. Yokochi, Y. Mizuno, N. Shimizu, Mutations in the parkin gene cause autosomal recessive juvenile parkinsonism, Nature 392 (1998) 605–608.

[4] E.M. Valente, P.M. Abou-Sleiman, V. Caputo, M.M. Muqit, K. Harvey, S. Gispert, Z. Ali, D. Del Turco, A.R. Bentivoglio, D.G. Healy, A. Albanese, R. Nussbaum, R. Gonzalez-Maldonado, T. Deller, S. Salvi, P. Cortelli, W.P. Gilks, D.S. Latchman, R.J. Harvey, B. Dallapiccola, G. Auburger, N.W. Wood, Hereditary early-onset Parkinson's disease caused by mutations in PINK1, Science 304 (2004) 1158–1160.

[5] V. Bonifati, P. Rizzu, F. Squitieri, E. Krieger, N. Vanacore, J.C. van Swieten, A. Brice, C.M. van Duijn, B. Oostra, G. Meco, P. Heutink, DJ-1(PARK7), a novel gene for autosomal recessive, early onset parkinsonism, Neurol Sci 24 (2003) 159–160.

[6] A. Ramirez, A. Heimbach, J. Grundemann, B. Stiller, D. Hampshire, L.P. Cid, I. Goebel, A.F. Mubaidin, A.L. Wriekat, J. Roeper, A. Al-Din, A.M. Hillmer, M. Karsak, B. Liss, C.G. Woods, M.I. Behrens, C. Kubisch, Hereditary parkinsonism with dementia is caused by mutations in ATP13A2, encoding a lysosomal type 5 P-type ATPase, Nat Genet 38 (2006) 1184–1191.

[7] A. Navarro, A. Boveris, Brain mitochondrial dysfunction and oxidative damage in Parkinson's disease, J Bioenerg Biomembr 41 (2009) 517–521.

[8] J. Zhu, C.T. Chu, Mitochondrial dysfunction in Parkinson's disease, J Alzheimers Dis 20 (Suppl. 2) (2010) S325–S334.

[9] S.J. Chinta, J.K. Andersen, Redox imbalance in Parkinson's disease, Biochim Biophys Acta 1780 (2008) 1362–1367.

[10] C. Zhou, Y. Huang, S. Przedborski, Oxidative stress in Parkinson's disease: a mechanism of pathogenic and therapeutic significance, Ann NY Acad Sci 1147 (2008) 93–104.

[11] D.G. Graham, Oxidative pathways for catecholamines in the genesis of neuromelanin and cytotoxic quinones, Mol Pharmacol 14 (1978) 633–643.

[12] P.J. Kahle, C. Haass, How does parkin ligate ubiquitin to Parkinson's disease? EMBO Rep 5 (2004) 681–685.

[13] F. Darios, O. Corti, C.B. Lucking, C. Hampe, M.P. Muriel, N. Abbas, W.J. Gu, E.C. Hirsch, T. Rooney, M. Ruberg, A. Brice, Parkin prevents mitochondrial swelling and cytochrome *c* release in mitochondria-dependent cell death, Hum Mol Genet 12 (2003) 517–526.

[14] J.J. Palacino, D. Sagi, M.S. Goldberg, S. Krauss, C. Motz, M. Wacker, J. Klose, J. Shen, Mitochondrial dysfunction and oxidative damage in parkin-deficient mice, J Biol Chem 279 (2004) 18614–18622.

[15] C.C. Stichel, X.R. Zhu, V. Bader, B. Linnartz, S. Schmidt, H. Lubbert, Mono- and double-mutant mouse models of Parkinson's disease display severe mitochondrial damage, Hum Mol Genet 16 (2007) 2377–2393.

[16] J.A. Botella, F. Bayersdorfer, F. Gmeiner, S. Schneuwly, Modelling Parkinson's disease in *Drosophila*, Neuromolecular Med 11 (2009) 268–280.

[17] J.C. Greene, A.J. Whitworth, I. Kuo, L.A. Andrews, M.B. Feany, L.J. Pallanck, Mitochondrial pathology and apoptotic muscle degeneration in *Drosophila* parkin mutants, Proc Natl Acad Sci USA 100 (2003) 4078–4083.

[18] M. Muftuoglu, B. Elibol, O. Dalmizrak, A. Ercan, G. Kulaksiz, H. Ogus, T. Dalkara, N. Ozer, Mitochondrial complex I and IV activities in leukocytes from patients with parkin mutations, Mov Disord 19 (2004) 544–548.

[19] K. Winkler-Stuck, F.R. Wiedemann, C.W. Wallesch, W.S. Kunz, Effect of coenzyme Q10 on the mitochondrial function of skin fibroblasts from Parkinson patients, J Neurol Sci 220 (2004) 41–48.

[20] H. Mortiboys, K.J. Thomas, W.J. Koopman, S. Klaffke, P. Abou-Sleiman, S. Olpin, N.W. Wood, P.H. Willems, J.A. Smeitink, M.R. Cookson, O. Bandmann, Mitochondrial function and morphology are impaired in parkin-mutant fibroblasts, Ann Neurol 64 (2008) 555–565.

[21] A. Grunewald, L. Voges, A. Rakovic, M. Kasten, H. Vandebona, C. Hemmelmann, K. Lohmann, S. Orolicki, A. Ramirez, A.H. Schapira, P.P. Pramstaller, C.M. Sue, C. Klein, Mutant Parkin impairs mitochondrial function and morphology in human fibroblasts, PLoS ONE 5 (2010) e12962.

[22] H. Deng, M.W. Dodson, H. Huang, M. Guo, The Parkinson's disease genes pink1 and parkin promote mitochondrial fission and/or inhibit fusion in *Drosophila*, Proc Natl Acad Sci USA 105 (2008) 14503–14508.

[23] M. Hochstrasser, Origin and function of ubiquitin-like proteins, Nature 458 (2009) 422–429.

[24] D. Mukhopadhyay, H. Riezman, Proteasome-independent functions of ubiquitin in endocytosis and signaling, Science 315 (2007) 201–205.

[25] B. Levine, Eating oneself and uninvited guests: autophagy-related pathways in cellular defense, Cell 120 (2005) 159–162.

[26] D. Narendra, A. Tanaka, D.F. Suen, R.J. Youle, Parkin is recruited selectively to impaired mitochondria and promotes their autophagy, J Cell Biol 183 (2008) 795–803.

[27] A.J. Whitworth, L.J. Pallanck, The PINK1/Parkin pathway: a mitochondrial quality control system? J Bioenerg Biomembr 41 (2009) 499–503.

[28] S.J. Cherra, C.T. Chu, Autophagy in neuroprotection and neurodegeneration: a question of balance, Future Neurol 3 (2008) 309–323.

[29] O. Rothfuss, H. Fischer, T. Hasegawa, M. Maisel, P. Leitner, F. Miesel, M. Sharma, A. Bornemann, D. Berg, T. Gasser, N. Patenge, Parkin protects mitochondrial genome integrity and supports mitochondrial DNA repair, Hum Mol Genet 18 (2009) 3832–3850.

[30] P. Puigserver, B.M. Spiegelman, Peroxisome proliferator-activated receptor-gamma coactivator 1 alpha (PGC-1 alpha): transcriptional coactivator and metabolic regulator, Endocr Rev 24 (2003) 78–90.

[31] J. St-Pierre, S. Drori, M. Uldry, J.M. Silvaggi, J. Rhee, S. Jager, C. Handschin, K. Zheng, J. Lin, W. Yang, D.K. Simon, R. Bachoo, B.M. Spiegelman, Suppression of reactive oxygen species and neurodegeneration by the PGC-1 transcriptional coactivators, Cell 127 (2006) 397–408.

[32] A. Di Fonzo, C.F. Rohe, J. Ferreira, H.F. Chien, L. Vacca, F. Stocchi, L. Guedes, E. Fabrizio, M. Manfredi, N. Vanacore, S. Goldwurm, G. Breedveld, C. Sampaio, G. Meco, E. Barbosa, B.A. Oostra, V. Bonifati, A frequent LRRK2 gene mutation associated with autosomal dominant Parkinson's disease, Lancet 365 (2005) 412–415.

[33] G.P. Dimri, X. Lee, G. Basile, M. Acosta, G. Scott, C. Roskelley, E.E. Medrano, M. Linskens, I. Rubelj, O. Pereira-Smith, et al., A biomarker that identifies senescent human cells in culture and in aging skin in vivo, Proc Natl Acad Sci USA 92 (1995) 9363–9367.

[34] G. Villani, G. Attardi, Polarographic assays of respiratory chain complex activity, Meth Cell Biol 80 (2007) 121–133.

[35] M. Greco, G. Villani, F. Mazzucchelli, N. Bresolin, S. Papa, G. Attardi, Marked aging-related decline in efficiency of oxidative phosphorylation in human skin fibroblasts, FASEB J 17 (2003) 1706–1708.

[36] A. Arnoldi, A. Tonelli, F. Crippa, G. Villani, C. Pacelli, M. Sironi, U. Pozzoli, M.G. D'Angelo, G. Meola, A. Martinuzzi, C. Crimella, F. Redaelli, C. Panzeri, A. Renieri, G.P.

Comi, A.C. Turconi, N. Bresolin, M.T. Bassi, A clinical, genetic, and biochemical characterization of SPG7 mutations in a large cohort of patients with hereditary spastic paraplegia, Hum Mutat 29 (2008) 522–531.
[37] G. Villani, M. Greco, S. Papa, G. Attardi, Low reserve of cytochrome *c* oxidase capacity in vivo in the respiratory chain of a variety of human cell types, J Biol Chem 273 (1998) 31829–31836.
[38] P. Sgobbo, C. Pacelli, I. Grattagliano, G. Villani, T. Cocco, Carvedilol inhibits mitochondrial complex I and induces resistance to H_2O_2-mediated oxidative insult in H9C2 myocardial cells, Biochim Biophys Acta 1767 (2007) 222–232.
[39] Y. Nochez, S. Arsene, N. Gueguen, A. Chevrollier, M. Ferre, V. Guillet, V. Desquiret, A. Toutain, D. Bonneau, V. Procaccio, P. Amati-Bonneau, P.J. Pisella, P. Reynier, Acute and late-onset optic atrophy due to a novel OPA1 mutation leading to a mitochondrial coupling defect, Mol Vis 15 (2009) 598–608.
[40] K.C. Lund, L.L. Peterson, K.B. Wallace, Absence of a universal mechanism of mitochondrial toxicity by nucleoside analogs, Antimicrob Agents Chemother 51 (2007) 2531–2539.
[41] S. Modica, A. Morgano, L. Salvatore, M. Petruzzelli, M.T. Vanier, R. Valanzano, D.L. Esposito, G. Palasciano, I. Duluc, J.N. Freund, R. Mariani-Costantini, A. Moschetta, Expression and localisation of insulin receptor substrate 2 in normal intestine and colorectal tumours. Regulation by intestine-specific transcription factor CDX2, Gut 58 (2009) 1250–1259.
[42] H.R. McLennan, M. Degli Esposti, The contribution of mitochondrial respiratory complexes to the production of reactive oxygen species, J Bioenerg Biomembr 32 (2000) 153–162.
[43] Z. Cao, Y. Li, Chemical induction of cellular antioxidants affords marked protection against oxidative injury in vascular smooth muscle cells, Biochem Biophys Res Commun 292 (2002) 50–57.
[44] C. Beauchamp, I. Fridovich, Superoxide dismutase: improved assays and an assay applicable to acrylamide gels, Anal Biochem 44 (1971) 276–287.
[45] R.L. Levine, D. Garland, C.N. Oliver, A. Amici, I. Climent, A.G. Lenz, B.W. Ahn, S. Shaltiel, E.R. Stadtman, Determination of carbonyl content in oxidatively modified proteins, Meth Enzymol 186 (1990) 464–478.
[46] T.F. Slater, B.C. Sawyer, The stimulatory effects of carbon tetrachloride and other halogenoalkanes on peroxidative reactions in rat liver fractions in vitro. General features of the systems used, Biochem J 123 (1971) 805–814.
[47] H. Schagger, T.A. Link, W.D. Engel, G. von Jagow, Isolation of the eleven protein subunits of the bc1 complex from beef heart, Meth Enzymol 126 (1986) 224–237.
[48] K. Nakaso, Y. Adachi, K. Yasui, K. Sakuma, K. Nakashima, Detection of compound heterozygous deletions in the parkin gene of fibroblasts in patients with autosomal recessive hereditary parkinsonism (PARK2), Neurosci Lett 400 (2006) 44–47.
[49] B.H. Robinson, R. Petrova-Benedict, J.R. Buncic, D.C. Wallace, Nonviability of cells with oxidative defects in galactose medium: a screening test for affected patient fibroblasts, Biochem Med Metab Biol 48 (1992) 122–126.
[50] D.P. Kelly, R.C. Scarpulla, Transcriptional regulatory circuits controlling mitochondrial biogenesis and function, Genes Dev 18 (2004) 357–368.
[51] J. Lin, C. Handschin, B.M. Spiegelman, Metabolic control through the PGC-1 family of transcription coactivators, Cell Metab 1 (2005) 361–370.
[52] C.B. Lucking, A. Durr, V. Bonifati, J. Vaughan, G. De Michele, T. Gasser, B.S. Harhangi, G. Meco, P. Denefle, N.W. Wood, Y. Agid, A. Brice, Association between early-onset Parkinson's disease and mutations in the parkin gene, N Engl J Med 342 (2000) 1560–1567.
[53] C. Aguiar Pde, P.S. Lessa, C. Godeiro Jr., O. Barsottini, A.C. Felicio, V. Borges, S.M. Silva, R.A. Saba, H.B. Ferraz, C.A. Moreira-Filho, L.A. Andrade, Genetic and environmental findings in early-onset Parkinson's disease Brazilian patients, Mov Disord 23 (2008) 1228–1233.
[54] M. Farrer, P. Chan, R. Chen, L. Tan, S. Lincoln, D. Hernandez, L. Forno, K. Gwinn-Hardy, L. Petrucelli, J. Hussey, A. Singleton, C. Tanner, J. Hardy, J.W. Langston, Lewy bodies and parkinsonism in families with parkin mutations, Ann Neurol 50 (2001) 293–300.
[55] P.P. Pramstaller, B. Kis, C. Eskelson, K. Hedrich, M. Scherer, E. Schwinger, X.O. Breakefield, P.L. Kramer, L.J. Ozelius, C. Klein, Phenotypic variability in a large kindred (Family LA) with deletions in the parkin gene, Mov Disord 17 (2002) 424–426.
[56] S.J. Lincoln, D.M. Maraganore, T.G. Lesnick, R. Bounds, M. de Andrade, J.H. Bower, J.A. Hardy, M.J. Farrer, Parkin variants in North American Parkinson's disease: cases and controls, Mov Disord 18 (2003) 1306–1311.
[57] R.P. Munhoz, D.S. Sa, E. Rogaeva, S. Salehi-Rad, C. Sato, H. Medeiros, M. Farrer, A.E. Lang, Clinical findings in a large family with a parkin ex3delta40 mutation, Arch Neurol 61 (2004) 701–704.
[58] C.A. Gautier, T. Kitada, J. Shen, Loss of PINK1 causes mitochondrial functional defects and increased sensitivity to oxidative stress, Proc Natl Acad Sci USA 105 (2008) 11364–11369.
[59] Y. Kuroda, T. Mitsui, M. Kunishige, M. Shono, M. Akaike, H. Azuma, T. Matsumoto, Parkin enhances mitochondrial biogenesis in proliferating cells, Hum Mol Genet 15 (2006) 883–895.
[60] B.C. Bowen, R.E. Block, J. Sanchez-Ramos, P.M. Pattany, D.A. Lampman, J.B. Murdoch, R.M. Quencer, Proton MR spectroscopy of the brain in 14 patients with Parkinson disease, AJNR Am J Neuroradiol 16 (1995) 61–68.
[61] D.T. Dexter, C.J. Carter, F.R. Wells, F. Javoy-Agid, Y. Agid, A. Lees, P. Jenner, C.D. Marsden, Basal lipid peroxidation in substantia nigra is increased in Parkinson's disease, J Neurochem 52 (1989) 381–389.
[62] E. Dalfo, M. Portero-Otin, V. Ayala, A. Martinez, R. Pamplona, I. Ferrer, Evidence of oxidative stress in the neocortex in incidental Lewy body disease, J Neuropathol Exp Neurol 64 (2005) 816–830.
[63] R.J. Castellani, G. Perry, S.L. Siedlak, A. Nunomura, S. Shimohama, J. Zhang, T. Montine, L.M. Sayre, M.A. Smith, Hydroxynonenal adducts indicate a role for lipid peroxidation in neocortical and brainstem Lewy bodies in humans, Neurosci Lett 319 (2002) 25–28.
[64] Z.I. Alam, S.E. Daniel, A.J. Lees, D.C. Marsden, P. Jenner, B. Halliwell, A generalised increase in protein carbonyls in the brain in Parkinson's but not incidental Lewy body disease, J Neurochem 69 (1997) 1326–1329.
[65] E. Floor, M.G. Wetzel, Increased protein oxidation in human substantia nigra pars compacta in comparison with basal ganglia and prefrontal cortex measured with an improved dinitrophenylhydrazine assay, J Neurochem 70 (1998) 268–275.
[66] L.M. Ambani, M.H. Van Woert, S. Murphy, Brain peroxidase and catalase in Parkinson disease, Arch Neurol 32 (1975) 114–118.
[67] S.J. Kish, C. Morito, O. Hornykiewicz, Glutathione peroxidase activity in Parkinson's disease brain, Neurosci Lett 58 (1985) 343–346.
[68] R.A. Floyd, Antioxidants, oxidative stress, and degenerative neurological disorders, Proc Soc Exp Biol Med 222 (1999) 236–245.
[69] F. Camoes, N.A. Bonekamp, H.K. Delille, M. Schrader, Organelle dynamics and dysfunction: a closer link between peroxisomes and mitochondria, J Inherit Metab Dis 32 (2009) 163–180.
[70] H.K. Delille, R. Alves, M. Schrader, Biogenesis of peroxisomes and mitochondria: linked by division, Histochem Cell Biol 131 (2009) 441–446.
[71] A. Bagattin, L. Hugendubler, E. Muelle, A. Bagattin, L. Hugendubler, E. Mueller, Transcriptional coactivator PGC-1{alpha} promotes peroxisomal remodeling and biogenesis, Proc Natl Acad Sci USA 107 (2010) 20376–20381.
[72] J.I. Koepke, K.A. Nakrieko, C.S. Wood, K.K. Boucher, L.J. Terlecky, P.A. Walton, S.R. Terlecky, Restoration of peroxisomal catalase import in a model of human cellular aging, Traffic 8 (2007) 1590–1600.
[73] J.I. Koepke, C.S. Wood, L.J. Terlecky, P.A. Walton, S.R. Terlecky, Progeric effects of catalase inactivation in human cells, Toxicol Appl Pharmacol 232 (2008) 99–108.
[74] S.R. Terlecky, J.I. Koepke, P.A. Walton, Peroxisomes and aging, Biochim Biophys Acta 1763 (2006) 1749–1754.
[75] D.P. Narendra, S.M. Jin, A. Tanaka, D.F. Suen, C.A. Gautier, J. Shen, M.R. Cookson, R.J. Youle, PINK1 is selectively stabilized on impaired mitochondria to activate Parkin, PLoS Biol 8 (2010) e1000298.
[76] C. Vives-Bauza, C. Zhou, Y. Huang, M. Cui, R.L. de Vries, J. Kim, J. May, M.A. Tocilescu, W. Liu, H.S. Ko, J. Magrane, D.J. Moore, V.L. Dawson, R. Grailhe, T.M. Dawson, C. Li, K. Tieu, S. Przedborski, PINK1-dependent recruitment of Parkin to mitochondria in mitophagy, Proc Natl Acad Sci USA 107 (2010) 378–383.
[77] S. Geisler, K.M. Holmstrom, D. Skujat, F.C. Fiesel, O.C. Rothfuss, P.J. Kahle, W. Springer, PINK1/Parkin-mediated mitophagy is dependent on VDAC1 and p62/SQSTM1, Nat Cell Biol 12 (2010) 119–131.
[78] J.Y. Lee, Y. Nagano, J.P. Taylor, K.L. Lim, T.P. Yao, Disease-causing mutations in parkin impair mitochondrial ubiquitination, aggregation, and HDAC6-dependent mitophagy, J Cell Biol 189 (2010) 671–679.
[79] P.K. Kim, D.W. Hailey, R.T. Mullen, J. Lippincott-Schwartz, Ubiquitin signals autophagic degradation of cytosolic proteins and peroxisomes, Proc Natl Acad Sci USA 105 (2008) 20567–20574.
[80] C.T. Chu, A pivotal role for PINK1 and autophagy in mitochondrial quality control: implications for Parkinson disease, Hum Mol Genet 19 (2010) R28–R37.
[81] L. Cui, H. Jeong, F. Borovecki, C.N. Parkhurst, N. Tanese, D. Krainc, Transcriptional repression of PGC-1alpha by mutant huntingtin leads to mitochondrial dysfunction and neurodegeneration, Cell 127 (2006) 59–69.
[82] R.K. Chaturvedi, N.Y. Calingasan, L. Yang, T. Hennessey, A. Johri, M.F. Beal, Impairment of PGC-1alpha expression, neuropathology and hepatic steatosis in a transgenic mouse model of Huntington's disease following chronic energy deprivation, Hum Mol Genet 19 (2010) 3190–3205.
[83] D. Marmolino, M. Manto, F. Acquaviva, P. Vergara, A. Ravella, A. Monticelli, M. Pandolfo, PGC-1alpha down-regulation affects the antioxidant response in Friedreich's ataxia, PLoS ONE 5 (2010) e10025.
[84] B. Zheng, Z. Liao, J.J. Locascio, K.A. Lesniak, S.S. Roderick, M.L. Watt, A.C. Eklund, Y. Zhang-James, P.D. Kim, M.A. Hauser, E. Grunblatt, L.B. Moran, S.A. Mandel, P. Riederer, R.M. Miller, H.J. Federoff, U. Wullner, S. Papapetropoulos, M.B. Youdim, I. Cantuti-Castelvetri, A.B. Young, J.M. Vance, R.L. Davis, J.C. Hedreen, C.H. Adler, T.G. Beach, M.B. Graeber, F.A. Middleton, J.C. Rochet, C.R. Scherzer, PGC-1alpha, a potential therapeutic target for early intervention in Parkinson's disease, Sci Transl Med 2 (2010) 52ra73.
[85] C. Canto, J. Auwerx, PGC-1alpha, SIRT1 and AMPK, an energy sensing network that controls energy expenditure, Curr Opin Lipidol 20 (2009) 98–105.
[86] K. Aquilano, P. Vigilanza, S. Baldelli, B. Pagliei, G. Rotilio, M.R. Ciriolo, Peroxisome proliferator-activated receptor gamma co-activator 1alpha (PGC-1alpha) and sirtuin 1 (SIRT1) reside in mitochondria: possible direct function in mitochondrial biogenesis, J Biol Chem 285 (2010) 21590–21599.
[87] I.H. Lee, L. Cao, R. Mostoslavsky, D.B. Lombard, J. Liu, N.E. Bruns, M. Tsokos, F.W. Alt, T. Finkel, A role for the NAD-dependent deacetylase Sirt1 in the regulation of autophagy, Proc Natl Acad Sci USA 105 (2008) 3374–3379.